Steel and Composite Structures, *Vol. 34, No. 6* (*2020*) *783-794*
DOI: https://doi.org/10.12989/scs.2020.34.6.783

Compressive behavior of rectangular sandwich composite wall with different truss spacings

Ying Qin*, Xin Chen, Wang Xi, Xing-Yu Zhu and Yuan-Ze Chen

Key Laboratory of Concrete and Prestressed Concrete Structures of Ministry of Education, School of Civil Engineering, Southeast University, Nanjing, China

(*Received October 23, 2019, Revised January 24, 2020, Accepted February 2, 2020*)

Abstract. Steel-concrete-steel sandwich composite wall is composed of two external steel plates and infilled concrete core. Internal mechanical connectors are used to enhance the composite action between the two materials. In this paper, the compressive behavior of a novel sandwich composite wall was studied. The steel trusses were applied to connect the steel plates to the concrete core. Three short specimens with different truss spacings were tested under compressive loading. The boundary columns were not included. It was found that the failure of walls started from the buckling of steel plates and followed by the crushing of concrete. Global instability was not observed. It was also observed that the truss spacing has great influence on ultimate strength, buckling stress, ductility, strength index, lateral deflection, and strain distribution. Three modern codes were introduced to calculate the capacity of walls. The comparisons between test results and code predictions show that AISC 360 provides significant underestimations while Eurocode 4 and CECS 159 offer overestimated predictions.

Keywords: truss spacing; sandwich composite wall; compressive behavior; strength

1. Introduction

Reinforced concrete walls are conventionally applied as the structural components to resist gravity loads in civil engineering (Chao *et al.* 2019). However, large gravity loads sometimes result in thick cross sections at the lower stories of the buildings. Brittle cracks of concrete under compressive loading are another concern for designers (Sakr *et al.* 2017).

Recently, steel-concrete-steel sandwich composite walls have been receiving wide attraction. A typical sandwich composite wall consists of a concrete core attached by two steel plates on both sides. Mechanical connectors or adhesive materials are used to enhance the composite action between the two materials. Sandwich composite wall offers several structural merits over conventional concrete wall in terms of high strength and ductility. It also exhibits superior structural behavior over steel plate with higher axial stiffness and less steel consumption (Massumi *et al.* 2018). The thin steel plates in composite walls are vulnerable to local buckling. Liang *et al.* (2003, 2004) developed finite element models to investigate the local and post-local buckling of steel plates in double skin composite walls under different loading conditions. Critical buckling interaction curves were developed for the strength design of the walls.

Extensive studies have been conducted to investigate the behavior of structural components under different types of loads. Seismic performance of structures is important to ensure the energy dissipation capacity during an earthquake and has been evaluated by Shahab *et al.* (2011) and Mirtaheri *et al.* (2012). Meanwhile, incremental dynamic analysis (IDA) is commonly applied to develop performance-based earthquake engineering design (Asgarian *et al.* 2012). Recently, endurance time analysis (ETA) has been proposed to predict the structural performance with less computational time and comparable accuracy compared with IDA (Hariri-Ardebili *et al.* 2014).

As the vertical component to resist gravity load in building, gravity seawall, and nuclear facility, the compressive behavior of sandwich composite walls should be investigated to ensure the structural behavior and safety. The literature review shows that most of the previous experimental studies on compression focused on the wall with profiled steel sheeting. Wright (1998) reported the axial behavior of sandwich composite wall system with profiled steel sheeting. It was found that both steel and concrete did not reach their full yield stress due to buckling of thin steel plates and inability of profiled shape of concrete. Hilo *et al.* (2016) developed a finite element model to simulate the axial load behavior of the wall proposed by Wright (1998). Mydin and Wang (2011) and Prabha *et al.* (2013) extended the research to the application of lightweight foamed concrete. Effective width method was introduced to predict the load-carrying capacity of the profiled sandwich wall. Meanwhile, limited research was done on the compressive behavior of sandwich composite walls with flat steel plate. Choi *et al.* (2014) presented the compressive behavior of sandwich composite wall with shear studs using ordinary and eco-oriented cement concrete. Simplified rules were proposed to evaluate the

*Corresponding author, Associate Professor
E-mail: qinying@seu.edu.cn

ISSN: 1229-9367 (Print), 1598-6233 (Online)

buckling strength of steel plate. Huang and Liew (2016) conducted a series of compression tests on sandwich composite walls with J-hook connectors. Nonlinear finite element model was established to predict the load-displacement responses, ultimate capacity, and failure modes of the walls.

Appropriate load transfer devices are needed in order to mobilize the composite action. Different mechanical connectors have been studied by several researchers. Shear studs (Yang *et al.* 2016, Bruhl and Varma 2017, Yan *et al.* 2018) were the most commonly applied connectors to bond the steel plates to concrete core. To further improve the structural behavior of the wall, Luo *et al.* (2015) used additional connecting bolts to tight the steel plates to the concrete core. Similarly, Ji *et al.* (2017) used additional tie bars and U-shaped bars to connect the two external steel plates. The research by Eom *et al.* (2009) adopted the sandwich composite wall using embedded shear bars. Nie *et al.* (2013), Chen *et al.* (2015), and Huang *et al.* (2018) developed steel diaphragm, distributed batten plates, and transverse stiffeners to achieve the concrete-steel boning in sandwich composite walls. Huang and Liew (2016) focused on the application of wall as slim offshore deck and developed J-hook connectors for sandwich composite wall with thickness less than 100 mm. Yan *et al.* (2019) proposed to use novel enhanced C-channel connectors.

Previous research showed that walls experienced severe damage at the locations of the connectors due to the stress and strain concentration. In addition, composite wall with headed studs of embedded bars is vulnerable to separation between steel plates and concrete core due to insufficient pull-out strength of connectors. Recently, a novel mechanical connector, namely steel truss, was used to bond the steel plates to concrete core (Qin *et al.* 2019). The steel truss was composed of two angles serving as chord members and curl bar serving as web member. The configuration of the sandwich composite wall was illustrated in Fig. 1. The application of truss connectors offers several advantages. Firstly, the trusses are welded to the interior face of steel plates by automatic machines rather than by workers, which is time saving and cost efficient. Secondly, the two steel plates are easy to locate at the right position after the trusses have been attached. Thirdly, the constructed steel plates, together with truss connectors, are convenient to be divided into several modules and delivered to the site to erect. Fourthly, the steel trusses are able to provide strong support to steel plates and prevent the steel plate from buckling outwards when pouring concrete.

Qin *et al.* (2019) conducted compressive tests on long walls (with the height of 3000 mm) with the considered parameter of truss spacing. The results showed that the failure mode was dominated by global instability. Furthermore, the boundary columns were included in previous study. In order to exclude the influence of overall buckling and boundary columns, in this research, three short sandwich composite walls without boundary enforcement were tested under compressive loading. The purpose was to further investigate the effect of truss spacing on the entire cross sectional capacity of the novel composite walls.

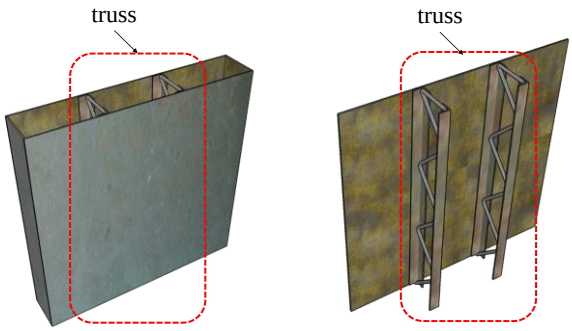

Fig. 1 Configuration of proposed sandwich composite wall

2. Experimental program

2.1 Optimization of truss connectors

The structural behavior of truss connectors is essential to ensure the compressive behavior of composite walls. Therefore, the dimensions of truss connectors should be optimized before the preparation of test. Finite element models were established using commercial software ANSYS. In the finite element models, the dimensions of the composite walls remained the same. The wall was 500 mm high, 900 mm wide, and 150 mm thick. The truss spacing was selected as 200 mm for all models. The key variables considered were the width and thickness of angles, the diameter of curl bar, and the vertical spacing of welding points for curl bar. The detailed information of the studied finite element models was given in Table 1.

The concrete was simulated by eight-node 3D solid element SOLID 65. The steel plates and the angles were simulated by the twenty-node solid element SOLID95. The curl bars were simulated by the 3D two-node finite strain linear beam element BEAM 188. The contact between steel plates and concrete core was modelled by TARGET170 and CONTA174.

Table 1 Details of the finite element models

FE model No.	B_t	t_t	d_b	d_t	Variable
	mm	mm	mm	mm	
B40T4D8V150	40	4	8	150	Control model
B30T4D8V150	30	4	8	150	Angle width
B50T4D8V150	50	4	8	150	Angle width
B40T2D8V150	40	2	8	150	Angle thickness
B40T6D8V150	40	6	8	150	Angle thickness
B40T4D6V150	40	4	6	150	Curl bar diameter
B40T4D10V150	40	4	10	150	Curl bar diameter
B40T4D8V100	40	4	8	100	Vertical spacing
B40T4D8V200	40	4	8	200	Vertical spacing

Note: B_t and t_t are the width and thickness of angles; d_b is the diameter of curl bar; and d_t is vertical spacing of welding points for curl bar

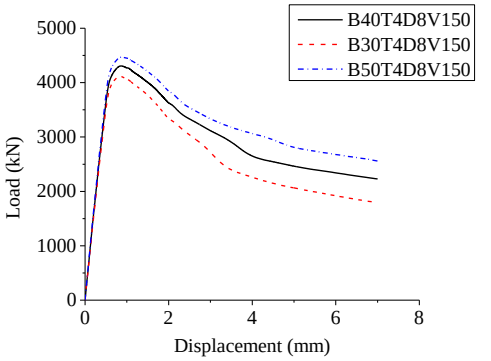

(a) Width of angles

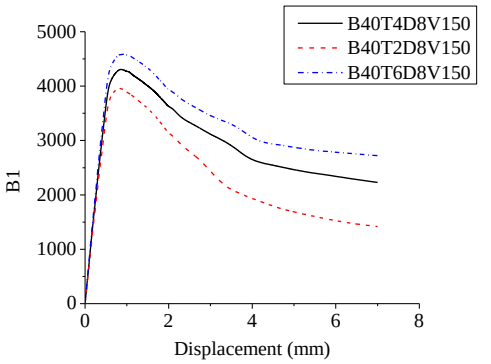

(b) Thickness of angles

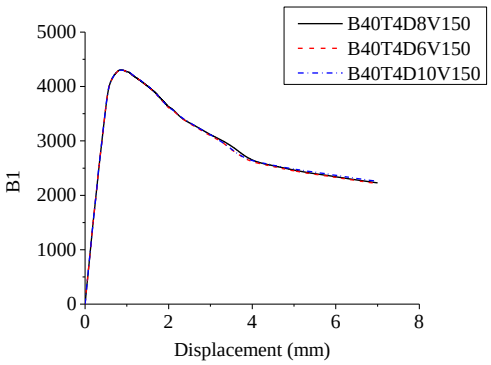

(c) Diameter of curl bar

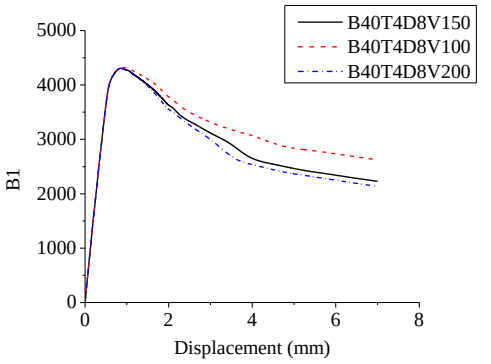

(d) Vertical spacing

Fig. 2 Axial load versus axial displacement curves for FE models

The material properties of steel and concrete were based on GB50017-2017 (2017) and GB50010-2010 (2010), respectively.

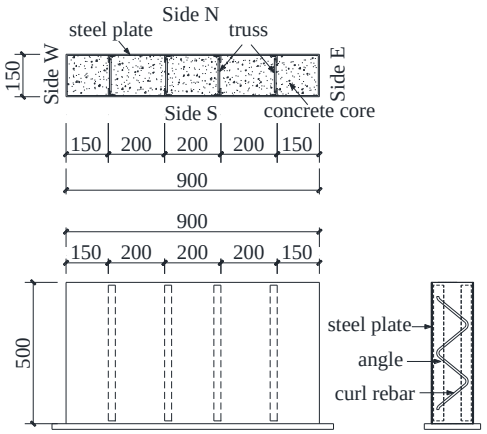

(a) Specimen W-200

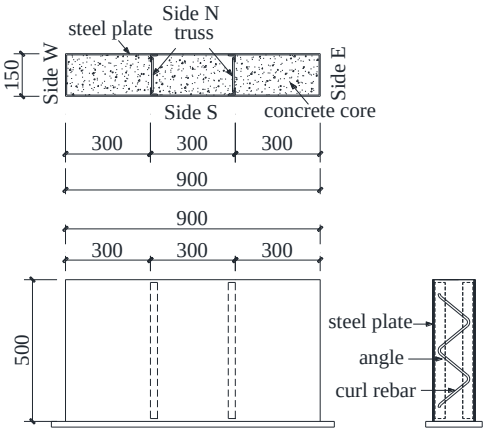

(b) Specimen W-300

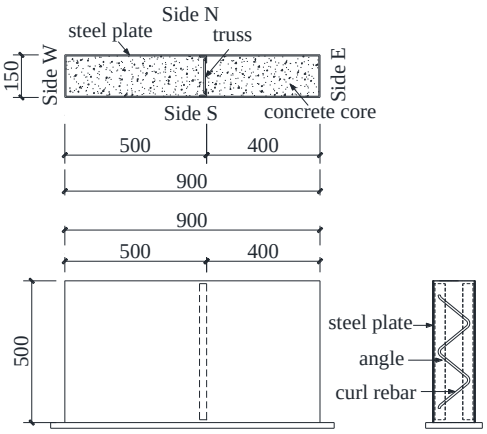

(c) Specimen W-400

Fig. 3 Tested specimens

Table 2 Specimen details

Specimen No.	h_w	L_w	b_w	t_s	d_s
	mm	mm	mm	mm	mm
W-200	500	900	150	4	200
W-300	500	900	150	4	300
W-400	500	900	150	4	400

Note: h_w, L_w and b_w are the height, length and width of sandwich composite wall; t_s is the thickness of steel plate; and d_s is the

truss spacing

The axial load versus axial displacement curves for all models were shown in Fig. 2. It can be seen that the influences of the diameter of curl bar and the vertical spacing of welding points for curl bar on the compressive behavior of composite walls are negligible. Meanwhile, the width and thickness of angles would affect the ultimate capacity of composite walls. The increase in both width and thickness of angles leads to the increase in ultimate capacity in almost linear manner. However, the initial stiffness was not significantly affected. Considering the availability of materials and the common dimension of angles in engineering practice, the angles were selected as L40×40×4 mm and the diameter of curl bar was selected as 8 mm.

2.2 Test specimens

Three specimens were designed in order to evaluate the compressive behavior of the sandwich composite walls. The details of the tested walls were shown in Fig. 3 and Table 2. All specimens had the same wall configuration. The height, length, and width of the wall were 500 mm, 900 mm, and 150 mm, respectively. The short height of the specimens means that the failure of the walls is expected to be dominated by cross-sectional capacity. The thickness of the external steel plates was 4 mm. Steel trusses were welded to the interior faces of the steel plates along the height of the wall.

While keeping the parameters above constant, the truss spacings were varied among three sandwich composite walls. The truss spacings for Specimens W-200, W-300, and W-400 were 200 mm, 300 mm, and 400 mm, respectively. The corresponding spacing-thickness ratios were $50\sqrt{235/f_y}$, $75\sqrt{235/f_y}$, and $100\sqrt{235/f_y}$, respectively.

2.3 Material properties

The strength grade of steel plates was Q235 with nominal yield strength of 235 MPa, according to the Chinese standard for classification of steel structures (GB50017-2017 2017). Three coupons were cut and fabricated from the same batch of steel to obtain the actual material properties. The tested average yield strength, ultimate strength, and elastic modulus were 346.0 MPa, 364.8 MPa, and 1.99×10^5 MPa.

The strength grade of the concrete core of all specimens was C20 with the characteristic value of cubic strength of 20 MPa, according to the Chinese code for design of concrete structures (GB20010-2010 2010). It should be noted that low concrete strength was selected in this research. This is due to the limitation of loading capacity of test machine. However, the influence of concrete strength is limited on the studied purpose in this research. Three cubes were cast with the geometry of 150×150×150 mm to get the actual cubic compressive strength. The tested average cubic compressive strength was 23.9 MPa. Due to the poor curing condition, the reduction coefficient of 0.88 suggested by GB20010-2010 (2010) was adopted to determine the corresponding cylinder strength which was 16.0 MPa.

Fig. 4 Test setup

2.4 Test setup and loading history

The sandwich composite walls were tested under compressive loading with the 10000 kN testing machine at Southeast University, as shown in Fig. 4. Fine sand was paved at the top of the walls to ensure the compressive loading was transferred uniformly to the entire cross section. The load was applied at intervals of 500 kN and remained for five minutes in order to record the data and observe the deformation. The axial displacement of the specimens and the local buckling of steel plates were appropriately recorded during the tests.

2.5 Instrumentations

The arrangement of linear variable displacement transducers (LVDTs) was shown in Fig. 5. LVDTs D1-D4 were placed vertically at the bottom of the specimen to measure the axial shortening during the test. Six LVDTs (D5-D10) were horizontally installed to measure the lateral deformation.

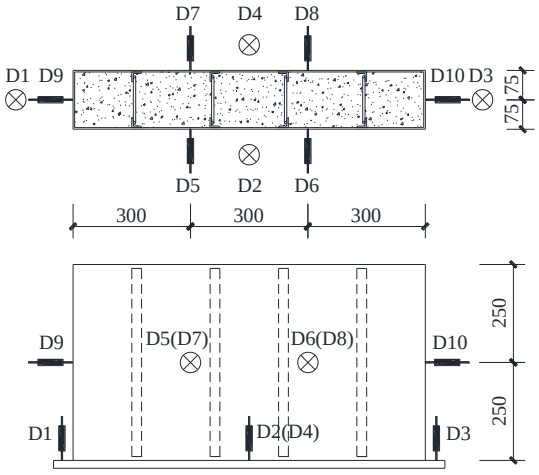

Fig. 5 Arrangement of displacement transducers

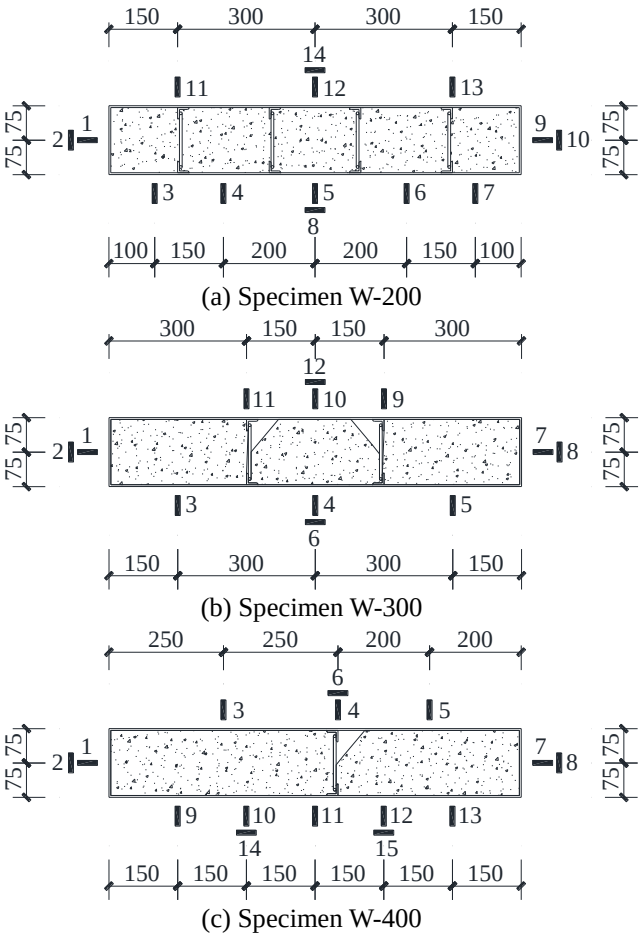

(a) Specimen W-200

(b) Specimen W-300

(c) Specimen W-400

Fig. 6 Arrangement of strain gauges

Fig. 6 shows the arrangement of strain gauges for three specimens. Strain gauges were arranged at the mid-height on the surface of the wall to monitor the strain development of the steel plates.

3. Experimental results and analysis

3.1 Failure mode

Fig. 7 shows the failure modes of the tested three specimens. Similar failure mode was observed from the tests, i.e., local buckling of steel plates, followed by the concrete crushing. Compared to long wall tested by Qin *et al.* (2019), global buckling failure mode was not found in these short wall specimens. It can also be found from Fig. 7 that the buckling waves occurred between the adjacent steel trusses. In addition, the buckling of specimen was more severe as the truss spacing increased. This means the steel truss was able to provide sufficient restraint to prevent the steel plates from buckling. Comparing with the test results of composite walls with shear studs (Choi *et al.* 2014, Yang *et al.* 2016) or J-hook connectors (Huang and Liew 2016), it can be found that the local buckling was postponed in composite wall with truss connectors, as the buckling occurred at a higher loading level in this test. Moreover, the buckling waves were slighter for composite walls with truss connectors, which further indicates the stronger restraint provided by truss connectors.

(a) Specimen W-200

(b) Specimen W-300

(c) Specimen W-400

Fig. 7 Failure modes

3.2 Load-axial displacement response

The compressive load versus axial shortening curves of the tested three sandwich composite walls were shown in

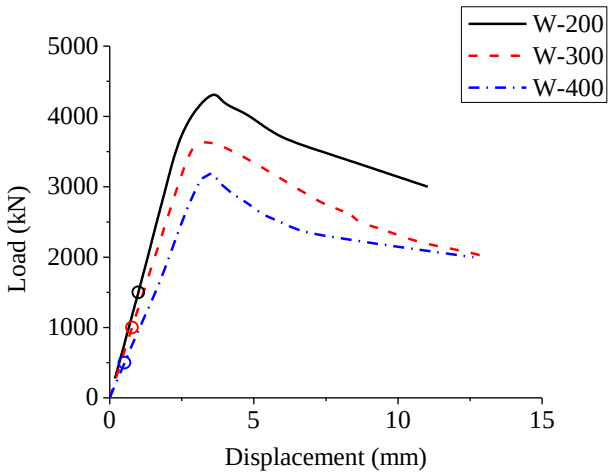

Fig. 8 Load-axial displacement curves

Fig. 8. It can be seen that the specimens experienced three different working stages, i.e., elastic stage, elastoplastic stage, and recession stage. The elastic stage started from the onset of loading and ended at the local buckling of steel plates. In this stage, the applied load on the specimen grew up linearly with the increase in the axial displacement. The elastoplastic stage started from the terminal point of elastic stage and ended at the point where the specimen reached its peak load. During this stage, the steel plates began to buckle outwards and the concrete exhibited nonlinear behavior. After that, in the third recession stage, specimen was not able to maintain its loading capacity due to severe concrete crushing and steel plate deforming. The reaction force gradually decreased with the increasing applied axial displacement. For specimens with smaller truss spacing, the sandwich composite walls experienced more ductile performance due to the better deformation ability of the steel plate.

3.3 Buckling stress

The thin steel plates in sandwich composite walls tend to exhibit local buckling when the walls are subjected to axial compressive load. However, due to the rigid contact with concrete core and the restraint offered by the truss connectors, the steel plates only buckle outwards with half-waves between the two adjacent truss connectors, as illustrated in Fig. 7. In order to determine the buckling strain and the corresponding buckling stress of the specimens, strain gauges were placed on steel plates to monitor the strain development. During the elastic stage, the values of strain are expected to be linearly increase as the applied load increases. When the steel plates start to buckle, the strain value will suddenly change at the location where local buckling occurs.

Fig. 9 shows the partially enlarged drawings of load-strain curves for several strain gauges in Specimens W-200, W-300, and W-400. The points where strain values abruptly change were marked by red squares. As can be seen from Fig. 9(a), Specimen W-200 has a buckling strain of 411 $\mu\varepsilon$, and the corresponding buckling stress and buckling load are 81.8 MPa and 1500 kN, respectively. The curves from Fig. 9(b) show that Specimen W-300 has a buckling strain of 86 $\mu\varepsilon$. The corresponding buckling stress and buckling load are 17.1 MPa 1000 kN, respectively. Fig. 9(c) shows that the buckling strain for Specimen W-400 is 72 $\mu\varepsilon$, and the corresponding buckling stress and buckling load are 14.3 MPa and 500 kN, respectively. The ratios of the buckling stress to the yield stress for Specimens W-200, W-300, and W-400 are 0.24, 0.05, and 0.04, respectively. The lowest ratio for Specimen W-400 demonstrates that the increase in the truss spacing weakens the restraint to the steel plates and leads to the reduction in the normalized buckling stress.

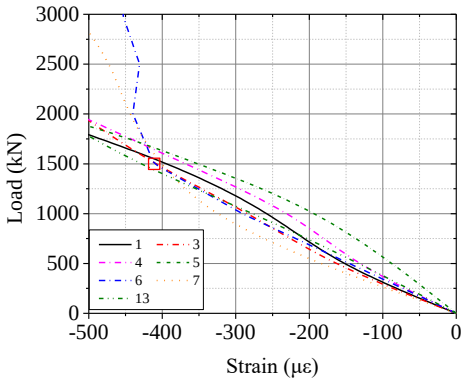

(a) Specimen W-200

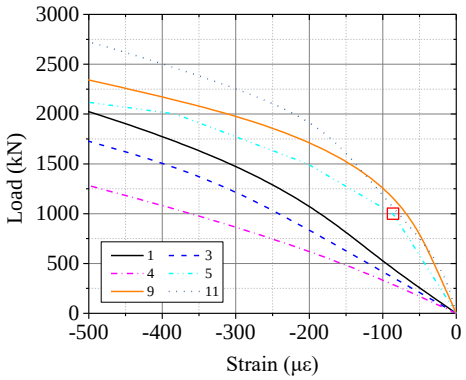

(b) Specimen W-300

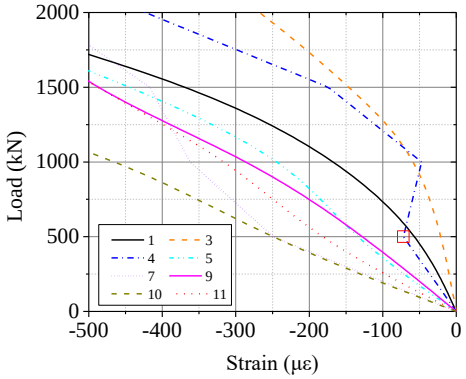

(c) Specimen W-400

Fig. 9 Determination of buckling strain

Previous research shows that the critical buckling stress of steel plate in composite wall is obtained when the effective width $\bar{B}$ is taken as the equivalent length, which can be expressed by Eq. (1) (Qin *et al.* 2017).

$$\sigma_{cr,Euler} = \frac{\pi^2 E_s}{12k^2(\bar{B}/t)^2} \quad (1)$$

A total of thirty-five composite walls with headed studs as the connectors were tested under compressive load by Akiyama and Sekimoto (1991), Usami *et al.* (1995), Kanchi (1996), and Choi and Han (2009). The relations between the normalized buckling strain $\varepsilon_{cr}/\varepsilon_y$ and the normalized slenderness ratio $\bar{B}/t \times \sqrt{f_y/E_s}$ of the data of these tests are given in Fig. 10. The data of Specimens W-200, W-300, and W-400 are also plotted. The blue solid line and red dash line are plotted based on Euler theory with k=1.0 and k=0.7, respectively.

It can be found that the data of Specimen W-200 is lying almost on the Euler line with k=1.0. This means that truss connectors provide a simple-supported boundary condition. On contrast, the data of Specimens W-300 and W-400 are even below the curve with k=1.0. This indicates that the truss spacing in these two specimens is too large to offer reasonable restraint to the steel plates. Compared to the previous research by Qin *et al.* (2019), it also shows that the boundary column has effective influence to help the truss connector better restrain the steel faceplate.

3.4 Ultimate strength and axial stiffness

The ultimate compressive strength of sandwich composite walls was obtained based on the load-axial displacement curves in Fig. 8. The determined ultimate strength N_u and the corresponding axial displacement d_u of the tested three specimens were given in Table 3. It can be observed that the ultimate strength of Specimens W-300 and W-400 were 13.6% and 25.0%, respectively, lower than that of Specimen W-200. The reduction in ultimate strength was mostly caused by the decrease in the buckling stress of steel plates.

The buckling load (N_b) and the corresponding displacement (d_b), the axial displacement corresponding to $0.3N_u$ ($d_{0.3u}$), and the axial displacement corresponding to $0.8N_u$ ($d_{0.8u}$) are tabulated in Table 3. The buckling loads were also marked in Fig. 8 by circles. It can be found in Fig. 8 that the slope of the load-displacement curves does not change obviously after reaching the buckling load. This indicated that the axial stiffness of the walls is not significantly affected by the buckling of steel plates.

In order to further identify the influence of plate buckling on the axial stiffness, two types of secant axial stiffness were used (Qin *et al.* 2019). The first (K_b) takes the point corresponding to buckling load as the starting point and the point corresponding to $0.8N_u$ as the terminal point, as expressed by Eq. (2). While the second ($K_{0.3u}$) takes the point corresponding to $0.3N_u$ as the starting point and the point corresponding to $0.8N_u$ as the terminal point, as shown in Eq. (3). As can be seen from Table 2, there are no significant differences in values between the two types of secant stiffness. This indicates that local buckling of steel plates does not obviously affect the axial stiffness. Meanwhile, it can be observed that the axial stiffness decreases with the increase in truss spacing, which is expected.

$$K_b = \frac{0.8N_u - N_b}{d_{0.8u} - d_b} \quad (2)$$

$$K_{0.3u} = \frac{0.8N_u - 0.3N_u}{d_{0.8u} - d_{0.3u}} \quad (3)$$

3.5 Ductility ratio

The ductility ratio (μ) is used to evaluate the ability of the sandwich composite wall to undergo large plastic deformation under compressive load without significant loss of strength. It is defined as the ratio of the axial displacement corresponding to 85% of the ultimate capacity during the recession stage ($d_{0.85u}$) to the displacement corresponding to ultimate capacity (d_u), and can be expressed as Eq. (4).

$$\mu = \frac{d_{0.85u}}{d_u} \quad (4)$$

The calculated ductility ratios for Specimens W-200, W-300, and W-400 are 1.69, 1.67, and 1.35, respectively. It can be found that the increase in truss spacing leads to the decrease in ductility. However, the value of ductility ratio only slightly decreases by 1% when the truss spacing increases from 200 mm to 300 mm, while the value sharply decreases by 19.2% as the truss spacing increases from 300 mm to 400 mm. This indicates that the truss spacing should be not greater than 300 mm in order to develop significant deformation while maintain sufficient capacity during the recession stage.

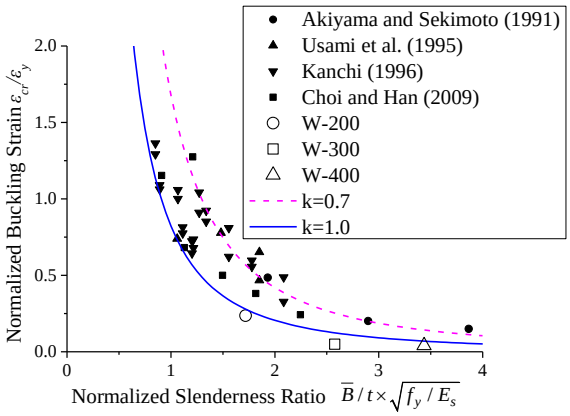

Fig. 10 Comparison with Euler theory

Table 3 Test results

Specimen	N_b	d_b	N_u	d_u	$d_{0.3u}$	$d_{0.8u}$	K_b	$K_{0.3u}$
	kN	mm	kN	mm	mm	mm	kN/mm	kN/mm
W-200	1500	0.99	4400	3.63	0.87	2.27	1578	1571
W-300	1000	0.77	3800	3.29	0.88	2.37	1275	1275
W-400	500	0.51	3300	3.47	1.02	2.64	1005	1019

3.6 Strength index

Strength index (*SI*) is essential to assess the bearing capacity and the composite action between the steel plates and concrete core. It can be defined by the ratio of the tested ultimate strength N_u to the fully-utilized capacity N_f, as shown in Eq. (5), where N_f can be calculated by Eq. (6). The calculated strength index for Specimens W-200, W-300, and W-400 are 0.90, 0.77, and 0.67, respectively. It can be found that strength index decreases with the increase in truss spacing. This indicates that the confinement effect of steel plates to concrete core becomes weaker as the truss spacing increases. Smaller truss spacing improves the composite action between steel and concrete and thus, enhances the bearing capacity.

$$SI = \frac{N_u}{N_f} \tag{5}$$

$$N_f = f_y A_s + f_c A_c \tag{6}$$

3.7 Load-lateral deformation response

The axial load versus lateral deformation responses of three specimens are given in Fig. 11. In the elastic stage, the lateral deformation for all specimens was quite small, and it slowly grew up with the increase in the compressive load. The slope of the load-lateral deformation curve for Specimen W-200 is the smallest while that for Specimen W-400 is the largest. This is because the ability to resist lateral deflection is better for wall with smaller truss spacing. In the elastoplastic stage, the slope of the curves gradually changed to a smaller value due to the buckling of steel plates or concrete crushing. After reaching the ultimate strength, the lateral deformation rapidly increases with the decrease of axial load.

3.8 Load-strain curves

Fig. 12 illustrates the load-strain curves for three specimens. The positive value means the tensile strain, while the negative value denotes the compressive strain. It can be seen that both the longitudinal and transverse strains almost increase linearly and slowly with the increase in compressive load during the initial loading stage. The increase rate becomes greater after the buckling of steel plates. In the recession stage, the strains develop quickly as the load continues to drop. Furthermore, the strain values of specimen with larger truss spacing are greater than that with smaller truss spacing at the same loading level, which also indicates that the truss connectors are effective in transferring part of axial load applied on steel plates to concrete core and thus prevent the early local buckling of steel plates.

Fig. 13 shows the strain distribution in three specimens under each loading level. During the first several loading steps, the strains are mostly distributed uniformly along the cross section. As the specimen is approaching its ultimate capacity, the non-uniformity of strain distribution starts to appear. It can also be noticed that the strains in specimen with smaller truss spacing are more uniform than those in specimen with larger truss spacing.

4. Code-based design

4.1 AISC 360-16

AISC 360-16 (2016) offers the calculation method to determine the compressive strength of axially loaded doubly symmetric filled composite members.

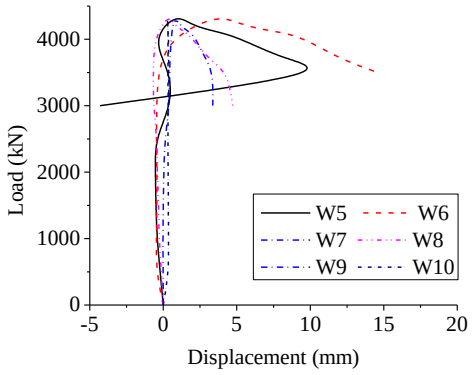

(a) Specimen W-200

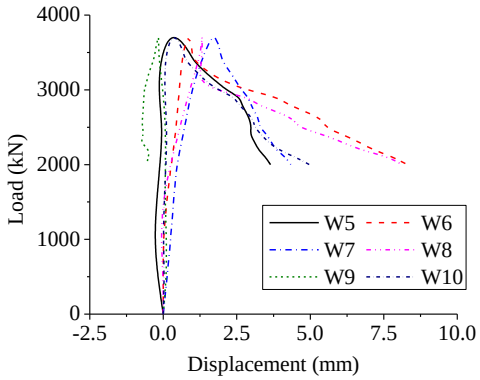

(b) Specimen W-300

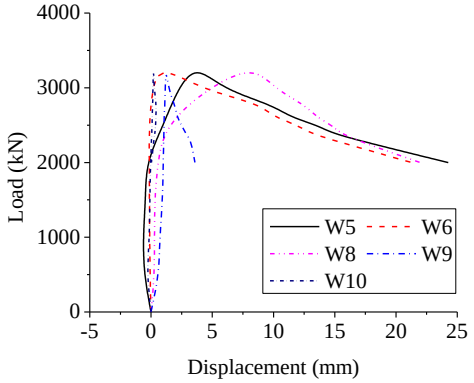

(c) Specimen W-400

Fig. 11 Load-lateral displacement curves

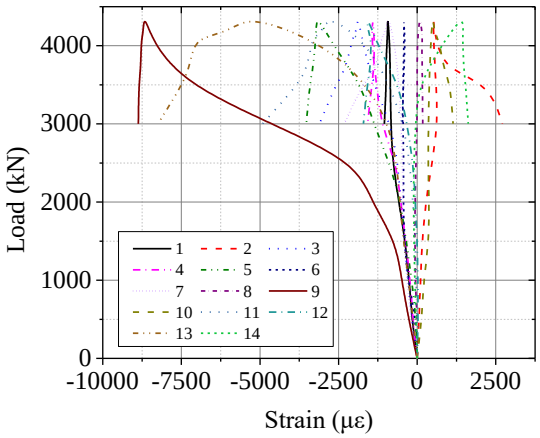

(a) Specimen W-200

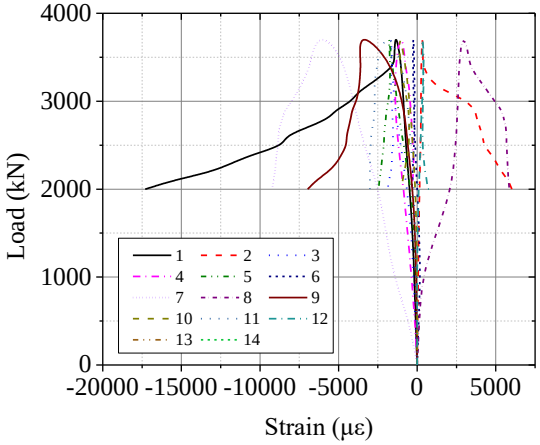

(b) Specimen W-300

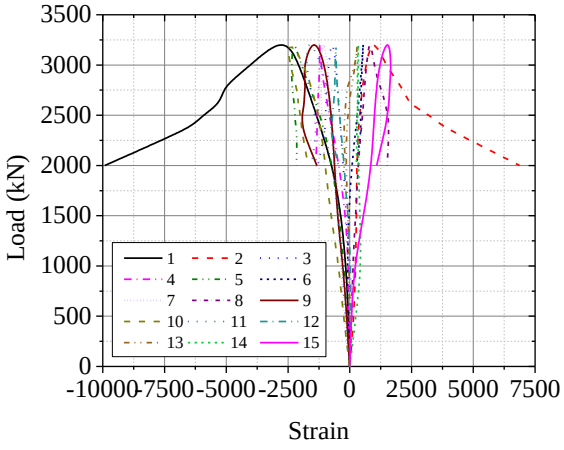

(c) Specimen W-400

Fig. 12 Load-strain curves

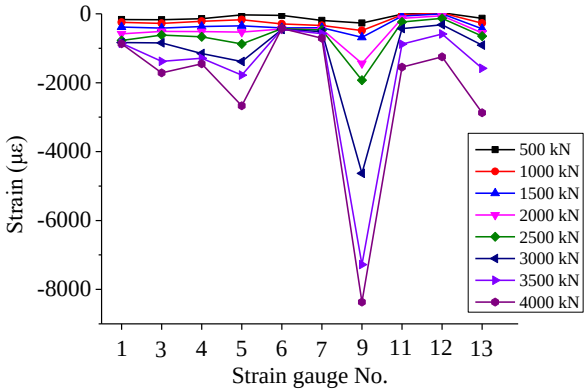

(a) Specimen W-200

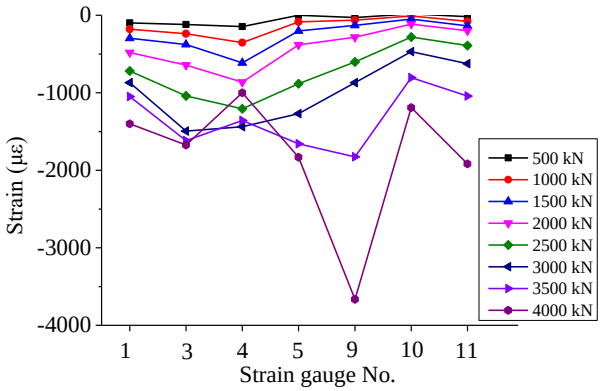

(b) Specimen W-300

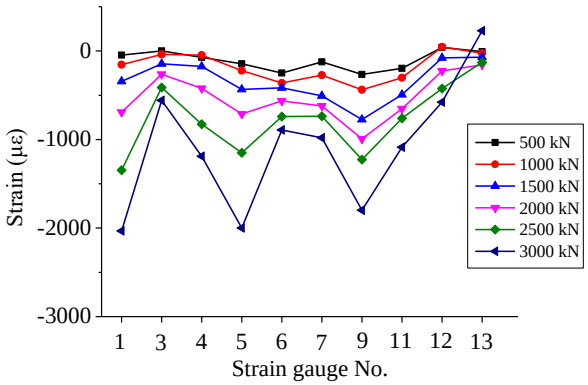

(c) Specimen W-400

Fig. 13 Strain distribution

For slender sections, the steel plates are considered to reach their buckling strength f_{cr} rather than their yield strength f_y. In addition, it is assumed that the steel is not able to provide sufficient confinement to the concrete core and thus the compressive strength of concrete core is reduced to $0.7f_c$. The expression is given by Eq. (7).

$$N_{AISC} = f_{cr}A_s + 0.7f_cA_c \tag{7}$$

where f_{cr} is the critical buckling stress of steel and can be obtained by Eq. (8) for rectangular filled sections, and other parameters have been previously defined.

$$f_{cr} = \frac{9E_s}{(b/t)^2} \tag{8}$$

4.2 EN 1994-1-1

Eurocode 4 (EN 1994-1-1, 2004) considers that the steel plate has ability to develop its yield stress of f_y. Meanwhile, the concrete core is well confined by the external steel plates and reaches its compressive strength of $0.85f_c$. The expression is shown in Eq. (9).

$$N_{EC4} = f_y A_s + 0.85 f_c A_c \quad (9)$$

4.3 CECS 159

CECS 159 (2004) uses the superposition principle to predict the strength of composite sections. It is assumed that the steel reaches its yield strength of f_y. In addition, concrete core reaches its compressive strength of f_c. The calculation method is expressed by Eq. (10).

$$N_{CECS} = f_y A_s + f_c A_c \quad (10)$$

4.4 Discussion

The comparison between the test data and the calculation results by modern codes are listed in Table 4. It should be mentioned that the cylinder compressive strength of concrete was used in the calculations of the wall strengths. Meanwhile, the capacity of the trusses is not included in the calculations of the wall strengths. It can be found that AISC 360-16 largely underestimates the actual capacity of sandwich composite walls. The average ratio of the test data to the predictions by the code is 2.44, and the corresponding standard deviation is 0.286. The great difference is because that AISC 360-16 underestimates the capacities of both steel and concrete. As can be seen from Fig. 11, the strains of steel are greater than the yielding strain when the specimen reaches its ultimate strength, which means the steel could develop fully yield strength in sandwich composite walls. In addition, due to the strong restraint offered by truss connectors, the steel plate is prevented from early local buckling and thus, is able to provide good confinement to concrete core. This enhances the compressive strength of concrete. It can also be observed that Eurocode 4 and CECS 159 offer unsafe predictions. For Eurocode 4, the average ratio of test results to predictions is 0.83 and the corresponding standard deviation is 0.098. While for CECS 159, the average ratio of test results to predictions is 0.78 and the corresponding standard deviation is 0.092.

Table 5 shows the predictions by three modern codes which included the capacity of the trusses in the calculations of the wall strengths. The ratios of the predicted results to the experimental results were also listed there. It can be found that the predicted capacity would increase when the contribution of truss connectors is taken into account. The increase rate is more quickly in Specimen W-200 than in the other two specimens, due to the fact that there are more trusses in Specimen W-200. The average ratios of the predicted results to the experimental results for AISC 360, Eurocode 4, and CECS 159 were 2.18, 0.75, and 0.71, respectively.

Table 4 Comparison with code-based predictions (exclude truss contribution)

Specimen No.	N_{AISC}	N_{EC4}	N_{CECS}	$\frac{N_u}{N_{AISC}}$	$\frac{N_u}{N_{EC4}}$	$\frac{N_u}{N_{CECS}}$
	kN	kN	kN			
W-200	1572	4607	4911	2.80	0.96	0.90
W-300	1572	4607	4911	2.42	0.82	0.77
W-400	1572	4607	4911	2.10	0.72	0.67
Average				2.44	0.83	0.78
Standard deviation				0.286	0.098	0.092

Table 5 Comparison with code-based predictions (include truss contribution)

Specimen No.	N_{AISC}	N_{EC4}	N_{CECS}	$\frac{N_u}{N_{AISC}}$	$\frac{N_u}{N_{EC4}}$	$\frac{N_u}{N_{CECS}}$
	kN	kN	kN			
W-200	1784	5415	5714	2.47	0.81	0.77
W-300	1753	5011	5312	2.17	0.76	0.72
W-400	1738	4809	5112	1.90	0.69	0.65
Average				2.18	0.75	0.71
Standard deviation				0.233	0.049	0.049

It can be seen from Tables 4 and 5 that Eurocode 4 and CECS 159 offer better predictions than AISC 360. This indicates that for this new type of composite wall, it is appropriate to assume the steel plate reaches its yield strength rather than buckling strength. This further shows that the truss connectors are effective in preventing premature local buckling. However, it also shows overestimations for Eurocode 4 and CECS 159. This may be caused by the fact that no boundary columns were employed and the compressive strength of concrete should be further reduced.

5. Conclusions

This research investigates the compressive behavior of a novel sandwich composite walls with steel trusses as the mechanical connectors. Compressive tests were conducted on three wall specimens with different truss spacings. The following conclusions are drawn based on the discussion in this research.

(1) The failure mode of the tested specimens includes the local buckling of steel faceplates and the subsequent cross-sectional capacity failure of the wall. No global instability was observed in the tests.

(2) The increase in truss spacing leads to the decrease in ultimate strength, buckling stress, axial stiffness, ductility, and strength index. In addition, greater truss spacing leads to larger lateral deflection under the same level of loading. The reduction in truss spacing could provide stronger restraint to steel plates and also results in more uniform

strain distribution. Meanwhile, the influence of local buckling on axial stiffness of wall can be ignored.

(3) AISC 360-16 significantly overestimates the capacity of walls, while Eurocode 4 and CECS 159 offer the unsafe predictions.

Acknowledgments

This work is sponsored by the Natural Science Foundation of Jiangsu Province (Grant No. BK20170685), and the National Key Research and Development Program of China (Grant No. 2017YFC0703802). The authors would like to thank the Zhejiang Southeast Space Frame Group Company Limited for the supply of test specimens.

References

AISC 360-16 (2016), Specification for structural steel buildings, American Institute of Steel Construction, Chicago, USA.

Akiyama, H. and Sekimoto, H. (1991), "A compression and shear loading tests of concrete filled steel bearing wall", *Transaction of 11th Structural Mechanics in Reactor Technology* (SMiRT-11), Tokyo, Japan, August.

Asgarian, B., Khazaee, H. and Mirtaheri, M. (2012), "Performance evaluation of different types of steel moment resisting frames subjected to strong ground motion through Incremental dynamic analysis", *Int. J. Steel Struct.*, **12**(3), 363-379. http://dx.doi.org/10.1007/s13296-012-3006-6.

Bruhl J.C. and Varma, A.H. (2017), "Experimental resistance and available ductility of steel-plate composite walls in one-way bending", *J. Struct. Eng.*, **143**(4), 04016222. http://dx.doi.org/10.1061/(ASCE)ST.1943-541X.0001714.

CECS 159 (2004), Technical specification for structures with concrete-filled rectangular steel tube members; China Association for Engineering Construction Standardization, Beijing, China.

Chao, S., Wu, H., Zhou, T., Guo, T. and Wang, C. (2019), "Application of self-centering wall panel with replaceable energy dissipation devices in steel frames", *Steel Compos. Struct.*, **32**(2), 265-279. http://dx.doi.org/10.12989/scs.2019.32.2.265.

Chen, L., Mahmoud, H., Tong, S.M. and Zhou, Y. (2015), "Seismic behavior of double steel plate–HSC composite walls", *Eng. Struct.*, **102**, 1-12. http://dx.doi.org/10.1016/j.engstruct.2015.08.017.

Choi, B.J. and Han, H.S. (2009), "An experiment on compressive profile of the unstiffened steel plate-concrete structures under compression loading", *Steel Comp. Struct.*, **9**(6), 519-534. https://doi.org/10.12989/scs.2009.9.6.519.

Choi, B.J., Kang, C.K. and Park, H.Y. (2014), "Strength and behavior of steel plate–concrete wall structures using ordinary and eco-oriented cement concrete under axial compression", *Thin Wall. Struct.*, **84**, 313-324. http://dx.doi.org/10.1016/j.tws.2014.07.008.

EN 1994-1-1 (2004), Eurocode 4: Design of composite steel and concrete structures-Part 1-1: General rules and rules for buildings, European Standard Institute, Brusels, Belgium.

Eom, T.S., Park, H.G., Lee, C.H., Kim, J.H. and Chang, I.H. (2009), "Behavior of double skin composite wall subjected to in-plane cyclic loading", *J. Struct. Eng.*, **135**(10), 1239-1249. http://dx.doi.org/10.1061/(ASCE)ST.1943-541X.0000057.

GB50010-2010 (2010), Code for design of concrete structures; China Architecture & Building Press, Beijing, China.

GB50017-2017 (2017), Standard for classification of steel structures; China Architecture & Building Press, Beijing, China.

Hariri-Ardebili, M.A., Rahmani-Samani, H. and Mirtaheri, M. (2014), "Seismic stability assessment of a high-rise concrete tower utilizing endurance time analysis", *Int. J. Struct. Stab. Dyn.*, **14**(6), 1450016. http://dx.doi.org/10.1142/S0219455414500163.

Hilo, S.J., Badaruzzaman, W.H.W., Osman, S.A. and Al-Zand, A.W. (2016), "Structural behavior of composite wall systems strengthened with embedded cold-formed steel tube", *Thin Wall. Struct.*, **98**, 607-616. http://dx.doi.org/10.1016/j.tws.2015.10.028.

Huang, S.T., Huang, Y.S., He, A., Tang, X.L, Chen, Q.J., Liu, X. and Cai, J. (2018), "Experimental study on seismic behaviour of an innovative composite shear wall", *J. Constr. Steel Res.*, **148**, 165-179. https://doi.org/10.1016/j.jcsr.2018.05.003.

Huang, Z.Y. and Liew, J.Y.R. (2016), "Compressive resistance of steel-concrete-steel sandwich composite walls with J-hook connectors", *J. Constr. Steel Res.*, **124**, 142-162. http://dx.doi.org/10.1016/j.jcsr.2016.05.001.

JGJ/T 380-2015 (2015), Technical specification for steel plate shear walls, China Architecture & Building Press, Beijing, China.

Kanchi, M. (1996), "Experimental study on a concrete filled steel structure Part 2 Compressive tests (1). Summary of Technical Papers of Annual Meeting", Architectural Institute of Japan, 1996, 1071-1072.

Liang, Q.Q., Uy, B., Wright, H.D. and Bradford, M.A. (2003), "Local and post-local buckling of double skin composite panels", *Proc. Inst. Civil Eng.-Struct. Build.*, **156**(2), 111-119.

Liang, Q.Q., Uy, B., Wright, H.D. and Bradford, M.A. (2004), "Local buckling of steel plates in double skin composite panels under biaxial compression and shear", *J. Struct. Eng.- ASCE*, **130** (3), 443-451. http://dx.doi.org/10.1061/(ASCE)0733-9445(2004)130:3(443).

Luo, Y.F., Guo, X.N., Li, J., Xiong, Z., Meng, L., Dong, N. and Zhang, J. (2015), "Experimental research on seismic behaviour of the concrete-filled double-steel-plate composite wall", *Adv. Struct. Eng.*, **18**(11), 1845-1858. http://dx.doi.org/10.1260/1369-4332.18.11.1845.

Massumi, A., Karimi, N. and Ahmadi, M. (2018), "Effects of openings geometry and relative area on seismic performance of steel shear walls", *Steel Compos. Struct.*, **28**(5), 617-628. http://dx.doi.org/10.12989/scs.2018.28.5.617.

Mirtaheri, S.M., Zandi, A.P., Mavandadi, S., Daryan, A.S. and Ziaei, M. (2012), "Study the possibility of seismic collision between adjacent structures: a case study of Karimkhan avenue in Tehran", *Des. Tall Spec. Build.*, **21**(3), 194-214. http://dx.doi.org/10.1002/tal.587.

Mydin, M.A.O. and Wang, Y.C. (2011), "Structural performance of lightweight steel-foamed concrete-steel composite walling system under compression", *Thin Wall. Struct.*, **49**, 66-76. http://dx.doi.org/10.1016/j.tws.2010.08.007.

Nie, J.G., Hu, H.S., Fan, J.S., Tao, M.X., Li, S.Y. and Liu, F.J. (2013), "Experimental study on seismic behavior of high-strength concrete filled double-steel-plate composite walls", *J. Constr. Steel Res.*, **88**, 206-219. http://dx.doi.org/10.1016/j.jcsr.2013.05.001.

Prabha, P., Marimuthu, V., Saravanan, M., Palani, G.S., Lakshmanan, N. and Senthil, R. (2013), "Effect of confinement on steel-concrete composite light-weight load-bearing wall panels under compression", *J. Constr. Steel Res.*, **81**, 11-19. http://dx.doi.org/10.1016/j.jcsr.2012.10.008.

Qin, Y., Shu, G.P., Fan, S.G., Lu, J.Y., Cao, S. and Han, J.H. (2017), "Strength of double skin steel-concrete composite walls", *Int. J. Steel Struct.*, **17**(2), 535-541. http://dx.doi.org/10.1007/s13296-017-6013-9.

Qin, Y., Shu, G.P., Zhou, G.G., Han, J.H. and Zhou, X.L. (2019), "Truss spacing on innovative composite walls under compression", *J. Constr. Steel Res.*, **160**, 1-15. https://doi.org/10.1016/j.jcsr.2019.05.027.

Sakr, M.A., El-Khoriby, S.R., Khalifa, T.M. and Nagib, M.T. (2017), "Modeling of RC shear walls strengthened by FRP composites", *Struct. Eng. Mech.*, **61**(3), 407-417. https://doi.org/10.12989/sem.2017.61.3.407.

Shahab, S., Mirtaheri, M., Mirzaeifar, R. and Bahai, H. (2011), "Modifying the shear buckling loads of metal shear walls for improving their energy absorption capacity", *Adv. Struct. Eng.*, **14**(6), 1247-1257. https://doi.org/10.1260/1369-4332.14.6.1247.

Usami, S., Akiyama, H., Narikawa, M., Hara, K., Takeuchi, M. and Sasaki, N. (1995), "Study on a concrete filled steel structure for nuclear plants (part 2). Compressive loading tests on wall members", *Transaction of 13th Structural Mechanics in Reactor Technology* (SMiRT-13), Porto Alegre, Brazil, August.

Wright, H. (1998), "The axial load behaviour of composite walling", *J. Constr. Steel Res.*, **45**(3), 353-375. https://doi.org/10.1016/S0143-974X(97)00030-8.

Yan, J.B., Wang, Z., Wang, T. and Wang, X.T. (2018), "Shear and tensile behaviors of headed stud connectors in double skin composite shear wall", *Steel Compos. Struct.*, **26**(6), 759-769. https://doi.org/10.12989/scs.2013.91.4.1301.

Yan, J.B., Chen, A.Z. and Wang, T. (2019), "Developments of double skin composite walls using novel enhanced C-channel connectors", *Steel Compos. Struct.*, **33**(6), 877-889. https://doi.org/10.12989/scs.2019.33.6.877.

Yang, Y., Liu, J.B. and Fan, J.S. (2016), "Buckling behavior of double-skin composite walls: An experimental and modeling study", *J. Constr. Steel Res.*, **121**, 126-135. http://dx.doi.org/10.1016/j.jcsr.2016.01.019.

BU